Research Article

Journal of Molecular Recognition

Received: 16 August 2012, Accepted: 9 October 2012, Published online in Wiley Online Library

(wileyonlinelibrary.com) DOI: 10.1002/jmr.2246

Protein–cofactor binding and ultrafast electron transfer in riboflavin binding protein under the spatial confinement of nanoscopic reverse micelles

Ranajay Saha, Surajit Rakshit, Pramod Kumar Verma, Rajib Kumar Mitra and Samir Kumar Pal*

In this contribution, we study the effect of confinement on the ultrafast electron transfer (ET) dynamics of riboflavin binding protein (RBP) to the bound cofactor riboflavin (Rf, vitamin B2), an important metabolic process, in anionic sodium *bis*(2-ethylhexyl) sulfosuccinate reverse micelles (AOT-RMs) of various hydration levels. Notably, in addition to excluded volume effect, various nonspecific interactions like ionic charge of the confining surface can influence the biochemical reactions in the confined environment of the cell. To this end, we have also studied the ET dynamics of RBP–Rf complex under the confinement of a cationic hexadecyltrimethylammonium bromide (CTAB) RMs with similar water pool size to the anionic AOT-RMs towards simulating equal restricted volume effect. It has been found that the spatial confinement of RBP in the AOT-RM of $w_0 = 10$ leads to the loss of its tertiary structure and hence vitamin binding capacity. Although, RBP regains its binding capacity and tertiary structure in AOT-RMs of $w_0 \geq 20$ due to its complete hydration, the ultrafast ET from RBP to Rf merely occurs in such systems. However, to our surprise, the ET process is found to occur in cationic CTAB-RMs of similar volume restriction. It is found that under the spatial confinement of anionic AOT-RM, the isoalloxazine ring of Rf is improperly placed in the protein nanospace so that ET between RBP and Rf is not permitted. This anomaly in the binding behaviour of Rf to RBP in AOT-RMs is believed to be the influence of repulsive potential of the anionic AOT-RM surface to the protein. Our finding thus suggests that under similar size restriction, both the hydration and surface charge of the confining volume could have major implication in the intraprotein ET dynamics in real cellular environments. Copyright © 2013 John Wiley & Sons, Ltd.

Keywords: riboflavin; riboflavin binding protein; electron transfer dynamics; confinement; hydration; surface charge of confinement; reverse micelles

INTRODUCTION

At the cellular interior, biopolymers such as proteins and DNA carry out various biological functions in a small space that can be approximated by nanosized confinement (or nanocavity). For example, DNA packs in virus capsids (Simpson *et al*., 2000) and orients in pores (Mathé *et al*., 2005), proteins fold in chaperonin cages (Brinker *et al*., 2001; Ellis and Minton, 2003) and ribosomal exit tunnels (Nissen *et al*., 2000). Altogether, reactions in such *in vivo* confined environments differ from those processes in a simple aqueous solution, and with recent advances in various computational/experimental methods and resources: investigations of macromolecular crowding and confinement effects on protein conformational changes (Cheung and Thirumalai, 2007; Homouz *et al*., 2009), folding (Munishkina *et al*., 2004; Ping *et al*., 2004; Zhou, 2004; Zhang and Cheung, 2007; Qin and Zhou, 2009), thermodynamics and kinetics of protein folding under confinement (Mittal and Best, 2008), its association (Minton, 1993; Griffin *et al*., 2005; Wang *et al*., 2009) and dynamics (Bernadó *et al*., 2004; McGuffee and Elcock, 2006) have deepened our understanding of biopolymer dynamics. Although considerable progress has been made in this direction of protein folding reaction, little is known about biochemical reaction dynamics like ultrafast electron transfer (ET) under cell-like confinement. ET is crucial to life and is ubiquitous in enzymatic catalysis (Bendall, 1996; Stubbe and van der Donk, 1998; Balzani, 2001), especially in enzymes with redox reactions (Sinnott, 1998). Flavoproteins with flavin chromophores are examples of such enzymes and are involved in various catalytic processes (Müller, 1991; Ghisla *et al*., 1999). The understanding of ET reaction dynamics of flavins in proteins and their redox reactions in cell-like confinement is crucial to the enzyme function.

In this contribution, we report the picosecond-resolved studies of ET dynamics of riboflavin (Rf; vitamin B2) in Rf-binding protein (RBP, a flavoprotein) under the confinement of sodium *bis*(2-ethylhexyl) sulfosuccinate reverse micelles (AOT-RMs) at various hydration levels (w_0 = [water]/[surfactant]). Encapsulation limits the available solvent, and the ability to precisely control micellar water

* *Correspondence to: Samir Kumar Pal, Department of Chemical, Biological and Macromolecular Sciences, S.N. Bose National Centre for Basic Sciences, Block JD, Sector III, Salt Lake, Kolkata 700098, India.*
E-mail: skpal@bose.res.in

R. Saha, S. Rakshit, P. K. Verma, R. K. Mitra, S. K. Pal
Department of Chemical, Biological and Macromolecular Sciences, S.N. Bose National Centre for Basic Sciences, Block JD, Sector III Salt Lake, Kolkata 700098, India

pool radius through hydration provides the flexibility to probe the effects of confinement in a systematic way. RM encapsulation is thus proposed to be an ideal model for crowded cellular confinement studies (Van Horn *et al*., 2009; Tian and Garcia, 2011; Yeung and Axelsen, 2012). Recently, it has been suggested that the dominant factors influencing protein behaviour *in vivo* are a combination of excluded volume effects and weak attractive forces (like hydrodynamic interactions and electrostatics) (Minton, 1983; Crowley *et al*., 2008; Li and Pielak, 2009; Jiao *et al*., 2010; Feig and Sugita, 2011). Nevertheless, how different electrostatic charge of the confining volumes affects protein–cofactor binding and the associated reaction dynamics like ultrafast ET has not been studied so far. To this end, we also monitor the ET dynamics of Rf in RBP under the confinement of a cationic hexadecyltrimethylammonium bromide (CTAB) RMs with similar water pool size to the anionic AOT-RMs towards simulating equal restricted volume effect. We have monitored the secondary and tertiary structures and the vitamin binding capacity of RBP at different hydration levels (w_0) of the RMs using various spectroscopic techniques like circular dichroism, UV-Vis absorption, steady-state and picosecond-resolved fluorescence studies. The different dynamics of ET observed in such environments has been correlated with the hydration and structure of the protein in the corresponding nanoconfining environments.

MATERIALS AND METHODS

RBP (Apo form) from chicken egg white (lyophilized powder) was purchased from Sigma. Rf (Sigma), CTAB (Fluka), isooctane (Spectrochem, 99.5%), sodium *bis*(2-ethylhexyl) sulfosuccinate salt (AOT; Fluka 99%), disodium hydrogen phosphate dehydrate (Sigma 99%) and sodium dihydrogen phosphate dehydrate (Sigma 99%) were used as received. Aqueous stock solutions of RBP were prepared in a phosphate buffer (10 mM) at pH 7.0 using double distilled water. The concentration of RBP in buffer was determined using the extinction coefficient value of 49000 M^{-1} cm^{-1} at 280 nm (Duyvis *et al*., 2002). Rf concentration was calculated from its absorbance using the extinction coefficient value of 12200 M^{-1} cm^{-1} at 450 nm (Duyvis *et al*., 2002). Unless otherwise mentioned, we have used 15 μM RBP and 7.5 μM Rf solutions for all the spectroscopic studies. Reverse micellar (RM) solutions were prepared by adding requisite volumes of aqueous solution of RBP or RBP–Rf complex into a given volume of surfactant solution (100 mM) in isooctane with gentle stirring to achieve RMs with required degree of hydration, w_0 (w_0 = [water] / [surfactant]). For CTAB-RM preparation, hexanol was additionally added as a cosurfactant in 1:9 ratios (v/v) to the isooctane solution.

Far-, near- and visible-UV circular dichroism (CD) measurements were performed on a JASCO 815 spectrometer. Far-UV CD studies were measured between 200 and 260 nm wavelength with protein concentration of 0.15 mg ml^{-1} using a cell of 0.1 cm path length. For the far-UV measurement, we used 50 mM AOT solution to avoid the noise in the CD spectrum due to the absorbance of RM in that region. Both near-UV and visible-UV CD measurements were made in 1.0 cm path length cell. Absorption and emission spectra were recorded with a Shimadzu UV-2450 spectrophotometer and a JobinYvon Fluoromax-3 fluorimeter, respectively. We used a commercially available picosecond diode laser-pumped (LifeSpec-ps) time-resolved fluorescence spectrophotometer from Edinburgh Instruments, UK, for time-resolved measurement. For 445 nm excitation, a diode laser from Edinburgh Instruments, UK, was used with instrument response function (IRF) of 80 ps. For RBP, we used a femtosecond-coupled time-correlated single-photon counting setup in which the sample was excited by the third harmonic laser beam (300 nm) of the 900 nm (0.5 nJ per pulse) using a mode-locked Ti-sapphire laser with an 80-MHz repetition rate (Tsunami, Spectra Physics), pumped by a 10-W Millennia (Spectra Physics) followed by a pulse-peaker (rate 8 MHz) and a third harmonic generator (Spectra-Physics, model 3980). The third harmonic beam was used for excitation of the sample inside the time-correlated single-photon counting instrument (IRF = 70 ps), and the second harmonic beam was collected as for the start pulse. Luminescence transients were fitted by a nonlinear least square fitting procedure to a function $\left(X(t) = \int_0^t E(t')R(t-t')dt'\right)$ comprising of the convolution of the IRF (E(t)) with a sum of exponentials $\left(R(t) = A + \sum_{i=1}^{N} B_i e^{-t/\tau_i}\right)$ with preexponential factors (B_i), characteristic lifetimes (τ_i) and a background (A). Relative concentration in a multiexponential decay was finally expressed as $c_n = \left(B_n / \sum_{i=1}^{N} B_i\right) \times 100$. The quality of the curve fitting is evaluated by reduced chi-square and residual data.

For the determination of hydrodynamic diameters of the RMs, dynamic light scattering (DLS) measurements were made with Nano-S Malvern instrument using a 4-mW He–Ne laser (λ = 632.8 nm). The size of the RM water pool was estimated by subtracting twice the molecular size of the surfactants (AOT = 1.1 nm and CTAB = 2.2 nm) from the respective measured diameter of the RM (assuming no solvent penetration) (Luisi and Magid, 1986).

RESULTS AND DISCUSSIONS

Figure 1a shows the absorption spectra of Rf bound to RBP in buffer and AOT-RMs of different degrees of hydration. Isoalloxazine ring is known to be responsible for the light absorption and emission of the flavin chromophore in the near-UV and visible regions (Choi and McCormick, 1980; Mataga *et al*., 2000). Although Rf absorbs mostly approximately at 450 nm, it also shows distinct absorbance in the 300-nm region (Figure 1a). The complexation of Rf with RBP in buffer is found to quench both the fluorescence of Rf (excited both at 300 and 445 nm) and tryptophan (Trp) fluorescence (excited at 300 nm) of protein (Figure 1b) compared with the free Rf and RBP in buffer, respectively (data not shown). The observed quenching of Rf upon binding with RBP in buffer is a consequence of ultrafast ET to the flavin chromophore (Rf) in the excited electronic state from nearby tryptophan or tyrosine residues present in RBP (Mataga *et al*., 2000; Zhong and Zewail, 2001; Lukacs *et al*., 2012; Rakshit *et al*., 2012). Upon confining RBP spatially in the AOT-RM of w_0 = 10, we find that Rf retains its characteristic fluorescence intensity at 520 nm (excited both at 300 and 445 nm; Figure 1b and its inset), which is characteristic of free Rf in buffer. However, in the AOT-RM of w_0 = 20 and 40, Rf fluorescence is quenched (Figure 1b and square symbol of Figure 1c), which is only observed when it binds to RBP and appears to mark the associated ET from RBP to Rf. The binding of Rf to RBP can similarly be concluded from the emission intensity (at 350 nm) of tryptophan residue of RBP, but this requires more

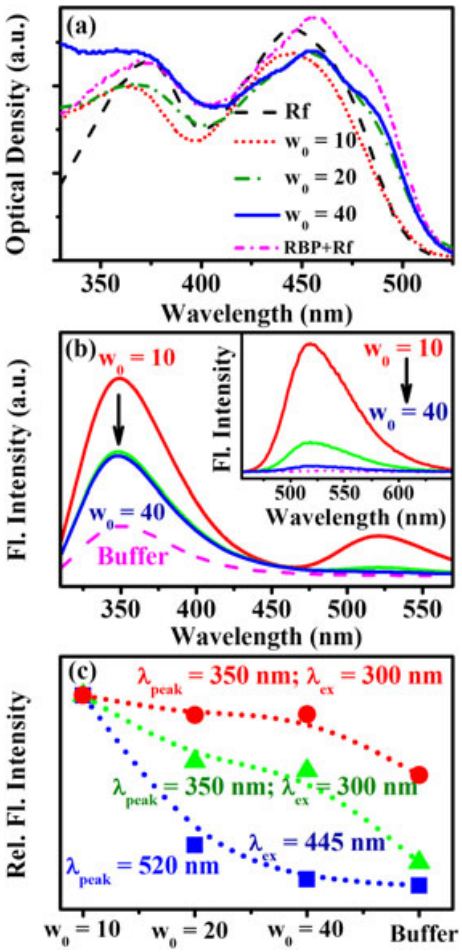

Figure 1. (a) Absorption spectra of RBP–Rf complex in buffer and AOT-RMs of $w_0 = 10$, 20 and 40. The black dashed line represents free Rf in buffer. (b) The total emission spectrum of the RBP–Rf complex in buffer and AOT-RMs of $w_0 = 10$, 20 and 40 ($\lambda_{ex} = 300$ nm). The inset shows the emission spectrum of the RBP–Rf complex excited at 445 nm in buffer (pink dotted line) and AOT-RMs of $w_0 = 10$, 20 and 40. (c) Relative fluorescence intensity of the Trp of RBP and RBP–Rf complex and the Rf of RBP–Rf complex in buffer and AOT-RMs of $w_0 = 10$, 20 and 40 (circle, RBP, $\lambda_{ex} = 300$ nm; triangle, RBP–Rf with $\lambda_{ex} = 300$ nm; square, RBP–Rf with $\lambda_{ex} = 445$ nm).

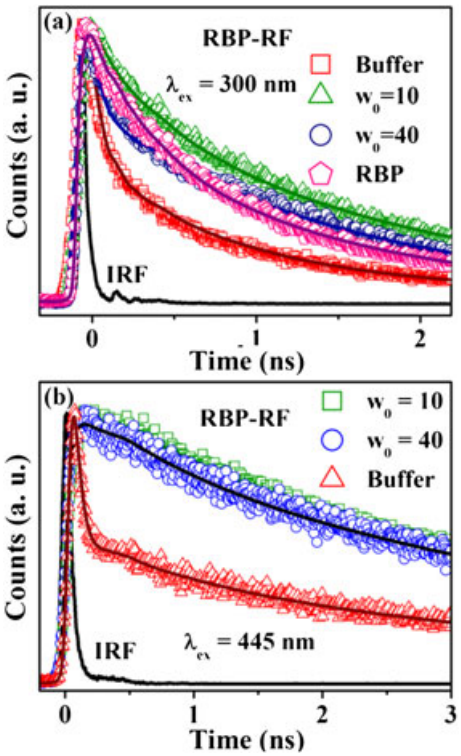

Figure 2. (a) Fluorescence decay transients of tryptophan of RBP–Rf complex ($\lambda_{ex} = 300$ nm; decay monitored at 350 nm) in buffer (square) and AOT-RMs of $w_0 = 10$ (triangle) and $w_0 = 40$ (circle). The pentagon represents free RBP decay in buffer. (b) Fluorescence decay transients of Rf of RBP–Rf complex ($\lambda_{ex} = 445$ nm; decay monitored at 520 nm) in buffer (triangle) and AOT-RMs of $w_0 = 10$ (square), $w_0 = 40$ (circle).

concern. Upon confining RBP in AOT-RM, we find that its fluorescence intensity ($\lambda_{em} = 350$ nm) increases in RM with decreasing w_0 values (Figure 1c, circular symbols), which might result from a change in the protein conformation due to confinement. On the other hand, in case of RBP–Rf complex, the fluorescence intensity of tryptophan residue increases in the AOT-RM of $w_0 = 10$ followed by substantial decrease in RM of $w_0 = 20$ and 40 (Figure 1c, triangular symbol). This quenching in tryptophan fluorescence in RM of $w_0 = 20$ and 40 could be related to Rf-binding in the protein nanospace and is believed to be both static and dynamic quenching discussed later.

To get a better insight into the observed change in fluorescence intensity, time-resolved fluorescence measurements are performed. Figure 2a shows the quenched decay transients of RBP–Rf complex (excited at 300 nm) in buffer compared with that of free RBP. The significant quenching of the Trp fluorescence is very much in line with the observed steady-state emission data discussed earlier (Figure 1b). Previously, Choi and McCormick (1980) suggested that the quenching of RBP fluorescence upon binding of Rf is mainly due to the ground-state stacking interaction between a Trp residue at the binding site and the quinoxaline portion. In fact, the distinct shift in the absorption peak position of RBP-bound Rf, compared with free Rf in buffer, supports such an explanation (Figure 1a). However, the significant quenching of Trp fluorescence in the excited state (Table 1) suggests that the quenching is dynamic in nature also. It is to be noted that considerable geometrical confinement of RBP (without Rf) in RM of $w_0 = 10$ leads to an increase in the average lifetime ($\langle\tau\rangle = a_1\tau_1 + a_2\tau_2 + a_3\tau_3$) of Trp residue (Table 1). However, increase in the water content of the RM reduces $\langle\tau\rangle$ of Trp to reach a value comparable with that obtained in buffer (Table 1). On the other hand, when RBP–Rf complex is confined in RM, the Trp lifetime in RM of $w_0 = 10$ system is found to be more or less comparable with that of RBP itself confined in RM of $w_0 = 10$, which clearly identifies the inability of RBP to bind Rf at this hydration level of RM. However, it is evident from Table 1 that for RBP–Rf complex in RM of $w_0 = 20$ and 40, $\langle\tau\rangle$ of Trp is quenched compared with that of RBP in RM with identical hydration, indicating that RBP is able to bind Rf in RM of $w_0 = 20$ and onwards.

The binding of Rf at a higher hydration of the protein is also evident in the absorbance (Figure 1a) and visible CD spectra (Figure 3c) of RBP–Rf complex in RM. In Figure 1a, it is observed that the bathochromic shift (~10 nm) in the visible band and a shoulder at ~490 nm, which is characteristic of Rf binding to RBP (Choi and McCormick, 1980), is absent in $w_0 = 10$ RM and is present in RM of $w_0 \geq 20$, indicating that RBP is able to bind Rf only in RM of $w_0 = 20$ and 40. Similarly, the appearance of strong CD bands in the visible region for RBP–Rf complex in RM of $w_0 = 20$ and 40 (Figures 3c and 3d) suggests Rf binding to RBP.

Table 1. Fluorescence lifetime components of RBP and RBP–Rf complex in buffer and different RMs

$\lambda_{ex} = 300$ nm, $\lambda_{em} = 350$ nm			a_1	τ_1 (ns)	a_2	τ_2 (ns)	a_3	τ_3 (ns)	$<\tau>$ (ns)
Buffer	—	RBP	0.49	0.24	0.43	1.18	0.08	3.64	0.92
	—	RBP–Rf	0.71	0.08	0.23	0.76	0.06	3.30	0.43
AOT-RM	$w_0 = 10$	RBP	0.33	0.24	0.54	1.50	0.13	4.44	1.47
	$w_0 = 20$		0.27	0.26	0.58	1.39	0.15	3.98	1.47
	$w_0 = 40$		0.42	0.16	0.47	1.35	0.11	4.23	1.17
	$w_0 = 10$	RBP–Rf	0.37	0.23	0.53	1.53	0.10	4.60	1.35
	$w_0 = 20$		0.37	0.21	0.54	1.42	0.09	4.21	1.22
	$w_0 = 40$		0.58	0.08	0.36	1.34	0.06	4.34	0.79
CTAB-RM	$w_0 = 25$	RBP	0.58	0.23	0.28	0.84	0.14	3.29	0.83
	$w_0 = 33$		0.58	0.21	0.28	0.78	0.14	3.22	0.78
	$w_0 = 25$	RBP–Rf	0.62	0.14	0.24	0.76	0.14	3.24	0.73
	$w_0 = 33$		0.60	0.14	0.27	0.68	0.13	3.33	0.69

τ_i represents decay time constant, a_i represents its relative contribution and $<\tau>$ is the average lifetime.

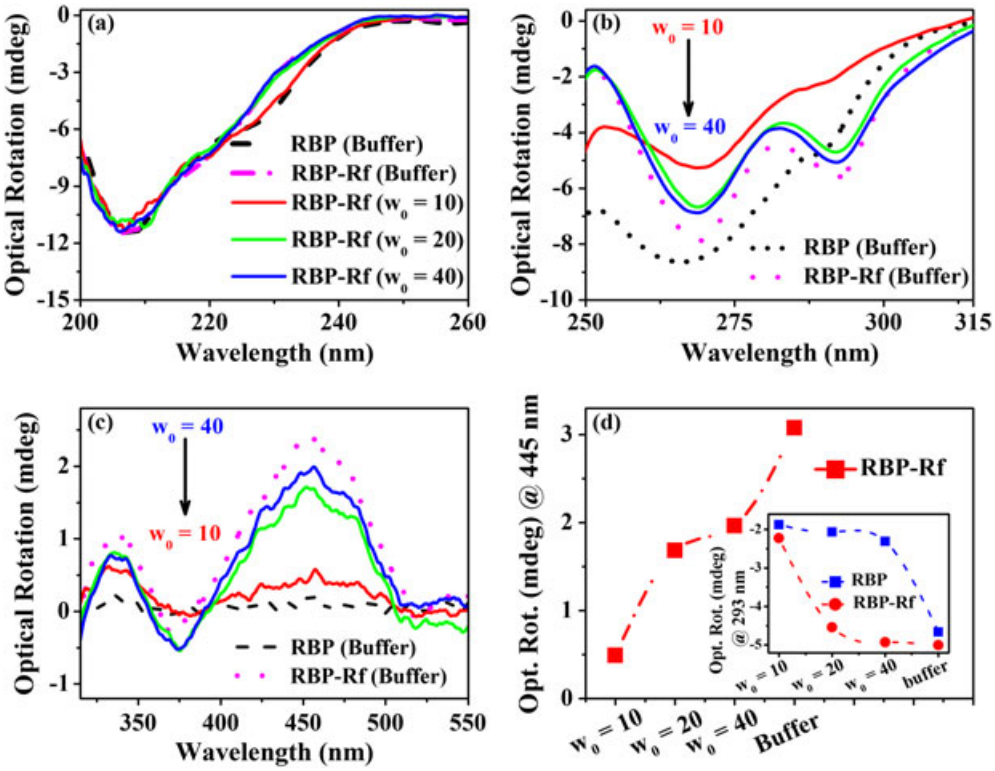

Figure 3. (a) Far-UV, (b) near-UV and (c) visible CD spectra of RBP in buffer and RBP–Rf complex in buffer, and AOT-RMs of $w_0 = 10$, 20 and 40. (d) Optical rotation value at 445 nm of RBP–Rf complex in buffer and AOT-RMs of $w_0 = 10$, 20 and 40. The inset shows the optical rotation value at 293 nm of RBP (square) and RBP–Rf (circle) in buffer and AOT-RMs of $w_0 = 10$, 20 and 40.

Importantly, the band positioned at ~445 nm is due to $\pi \rightarrow \pi^*$ transition, whereas those at 370 and 340 nm are attributed to a second $\pi \rightarrow \pi^*$ and $n \rightarrow \pi^*$ transitions, respectively (Figure 3c) (Galat, 1988). These strong CD bands suggest that Rf is rigidly packed in the binding cleft, and the rotation of the ribose moiety is completely hindered. It is important to mention here that the encapsulation of either RBP or RBP–Rf complex does not result in any significant change in the secondary structure (Figures 4a and 3a, respectively). However, the tertiary structure of the RBP–Rf complex as well as that of the protein itself suffers considerable perturbation upon confinement in $w_0 = 10$ RM system, as concluded from a loss in the intensity of the peaks at 268 and 293 nm (Figure 3b). With increased hydration ($w_0 \geq 20$), the near-UV CD spectrum considerably recovers its native form for the RBP–Rf complex, however, not for the protein itself (Figures 3b and inset of 3d). Indeed, one can observe that although the intensity of the CD signal for RBP at 293 nm is almost unaltered, it increases for the RBP–Rf complex with the increased hydration of the RM (Figure 3d, inset). This behaviour affirms that vitamin when bound to the protein indeed plays an important role in providing extra stability to protein in confined environment just like Rf-bound RBP has enhanced thermal stability manifested by the increase of denaturation temperature from 60.8°C to 72.8°C (Wasylewski, 2000).

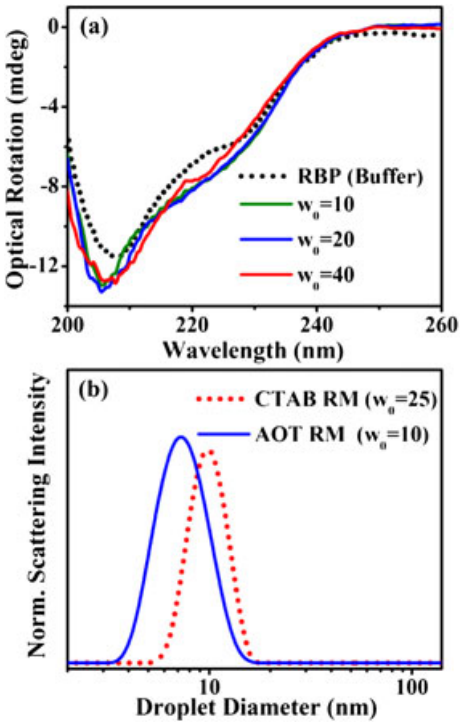

Figure 4. (a) Far-UV CD spectra of RBP in buffer and AOT-RMs of $w_0 = 10$, 20 and 40. (b) Representative DLS signals for AOT and CTAB-RMs.

The observations mentioned earlier might be better understood in terms of confinement and water properties in RM. Water present inside the RM can broadly be distinguished as bound type (water molecules hydrogen bonded to the interface) and bulk type (Verma *et al*., 2010; Saha *et al*., 2012). At very low w_0, the water molecules in the pool remain very close and strongly attracted to the polar head groups of the surfactants and hence are rather slow moving. As w_0 increases, the size of the water pool increases, and in such large water pools, the mobility of water molecules becomes relatively high. This change in mobility of the entrapped water molecules inside the RM has also been reported to affect the reaction kinetics occurring in the RM (Verma *et al*., 2009). In RM of $w_0 = 10$, RBP retains its secondary structure although loses its tertiary structure partially as well as its binding capability. It is important to note here that the presence of hydration shell is essential for a macromolecule's biological activity (Pal and Zewail, 2004). Without hydration water, proteins would lack not only their native folded structure but also the conformational flexibility that allows their biological activity (Rupley and Careri, 1991). For proteins with nearly spherical shape, the empirical relationship between its molar mass (M) and the hydration degree of RM is described by the following relation (Eryomin and Metelitza, 1999),

$$w_0 = (0.083 \pm 0.008)\sqrt{M} \quad (1)$$

Equation (1) indicates that the maximum degree of hydration for RBP ($M = 30$ kDa) is expected to occur at $w_0 = 13$–16. It seems that in $w_0 = 10$ AOT-RM, RBP is in a lower degree of hydration compared with that in aqueous buffer, making the protein relatively rigid and hence not functional. In RMs of $w_0 \geq 20$, the abundance of bulk type water compensates its dehydration and also geometrical confinement is relieved at a higher extent compared with that in $w_0 = 10$ RM, bringing in RBP's native tertiary structure and hence its functionality.

The complexation of Rf with RBP in buffer leads to the quenching of Rf fluorescence (Mataga *et al*., 2002), as also observed in Figure 1b. Although significant quenching in the steady-state fluorescence of Rf is observed upon binding with RBP in $w_0 = 20$ and 40 RM, its lifetime does not change appreciably (Figure 2b and Table 2). The unchanged fluorescence decay of Rf in RBP rules out the occurrence of ultrafast ET in AOT-RMs ($w_0 \geq 20$). As has been discussed earlier, RBP regains its tertiary structure and binding capacity in RMs of $w_0 \geq 20$. So quenching in the lifetime of Rf bound to RBP is expected in RM of $w_0 = 20$ and 40 (Figure 2b). Remarkably, ET and its rate are dependent on the redox centre distance (Isied *et al*., 1992; Winkler, 2006; Mondol *et al*., 2012), for example, tunnelling times range from a few nanoseconds (12.2 Å ET in the high-potential iron–sulfur protein from *Chromatium vinosum*) to 10 ms (26 Å ET in *Pseudomonas aeruginosa azurin*) (Winkler, 2006). For flavin chromophores with various flavoproteins, the ET rate is found to be different due to different chromophore-aromatic amino acid residue arrangements in the protein nanospace (Mataga *et al*., 2000). The donor–acceptor distance dependence of photoinduced ET in flavoproteins has been revealed by the work of Tanaka *et al*. (2007). In the confinement of AOT-RM ($w_0 \geq 20$), the nonoccurrence of ultrafast ET in the protein nanospace is thus

Table 2. Fluorescence lifetime components of Rf and RBP–Rf complex in buffer and different RMs

$\lambda_{ex} = 445$ nm, $\lambda_{em} = 520$ nm			a_1	τ_1 (ns)	a_2	τ_2 (ns)	a_3	τ_3 (ns)	$<\tau>$ (ns)
Buffer	—	Rf	0.00	1.00	0.00	1.00	1.00	4.70	4.70
	—	RBP–Rf	0.83	0.03	0.05	0.80	0.12	4.78	0.64
AOT-RM	$w_0 = 10$	Rf	0.20	1.11	0.00	1.00	0.80	4.84	4.09
	$w_0 = 20$		0.20	0.62	0.00	1.00	0.80	4.69	3.88
	$w_0 = 40$		0.15	0.79	0.00	1.00	0.85	4.72	4.13
	$w_0 = 10$	RBP–Rf	0.21	0.61	0.00	1.00	0.79	4.81	3.93
	$w_0 = 20$		0.20	0.65	0.00	1.00	0.80	4.81	3.98
	$w_0 = 40$		0.18	1.20	0.00	1.00	0.82	4.81	4.16
CTAB-RM	$w_0 = 25$	Rf	0.68	0.21	0.32	0.60	0.00	1.00	0.33
	$w_0 = 33$		0.76	0.27	0.24	0.81	0.00	1.00	0.40
	$w_0 = 25$	RBP–Rf	0.74	0.05	0.24	0.45	0.02	2.45	0.20
	$w_0 = 33$		0.73	0.05	0.24	0.52	0.03	2.44	0.23

τ_i represents decay time constant, a_i represents its relative contribution and $<\tau>$ is the average lifetime.

believed to be the improper distance between the donor and the acceptor pair because of the electrostatic charge interaction of the RM surface as discussed later. Remarkably, in a proper redox distance with aromatic amino acids in RBP, the near-UV absorption band position of Rf does not undergo any shift (Choi and McCormick, 1980). The combination of red shift by complexing with aromatic amino acids at the binding site and blue shift due to nonpolar environment in the protein nanospace results in nearly unshifted band position of Rf in RBP. However, in AOT-RMs of $w_0 \geq 20$, a small blue shift in the near-UV band position coupled with a shoulder at 490 nm (Figure 1a) suggests the improper complexation of Rf with the aromatic amino acids. In this context, the steady-state quenching of Trp fluorescence in AOT-RMs also needs some attention. Previously, the observed substantial quenching of Trp fluorescence (~65%, data not shown) in buffer was attributed to the presence of 5 out of 6 tryptophans in RBP in the vicinity (<0.45 nm) of Rf (Choi and McCormick, 1980). However, for AOT-RMs of $w_0 \geq 20$, such quenching of Trp fluorescence is found to be only ~40% (data not shown) compared with the free RBP in respective RMs. Thus, both steady-state absorption and emission spectroscopic data suggest the improper complexation of Rf for ET in the RBP interior, and in this condition, the observed steady-state quenching of Rf fluorescence in RM of $w_0 = 20$ and 40 systems is believed to be due to the ground-state stacking interaction of Rf with RBP.

To investigate the effect of confinement by a cationic surfactant forming RM, we chose CTAB-RMs with similar water pool size ($w_0 = 25$ and 33) to that of the AOT-RM of $w_0 = 10$ and 40, respectively (Table 3). Figure 4b is the representative DLS signals for each AOT and CTAB-RMs. The DLS signals are indicative of

Table 3. DLS data of AOT and CTAB-RMs of various w_0 values

AOT-RM			CTAB-RM		
w_0	Droplet diameter (nm)	Water pool size (nm)	w_0	Droplet diameter (nm)	Water pool size (nm)
5	6.70	4.50	10	6.10	1.90
10	7.56	5.36	20	8.40	4.20
20	10.06	7.86	25	9.90	5.70
40	14.90	12.70	30	14.4	10.2
—	—	—	35	22.2	18.0
—	—	—	40	24.0	20.3

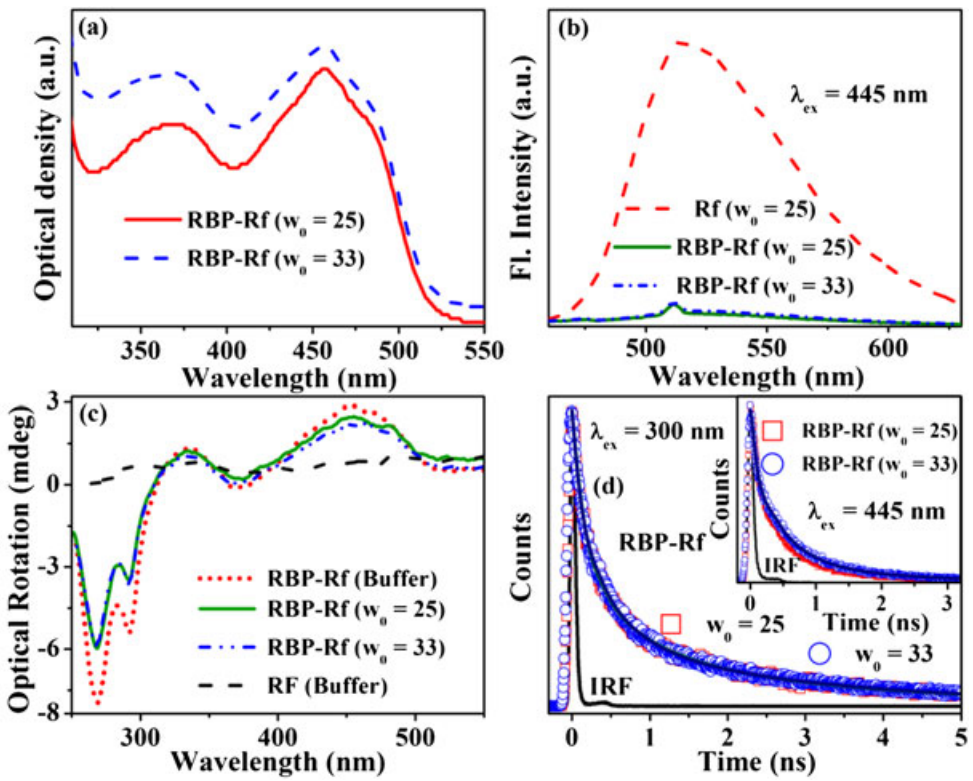

Figure 5. (a) Absorption spectra of RBP–Rf complex in CTAB-RMs of $w_0 = 25$ and 33. (b) Emission spectra of free Rf and RBP–Rf complex in CTAB-RMs of various w_0 values ($\lambda_{ex} = 445$ nm). (c) Visible CD spectra of Rf and RBP–Rf complex in buffer, and CTAB-RMs of $w_0 = 25$ and 33. (d) Fluorescence decay transients of tryptophan of RBP–Rf complex ($\lambda_{ex} = 300$; decay monitored at 350 nm) in CTAB-RMs of $w_0 = 25$ (square) and 33 (circle). The inset shows decay transient of Rf of RBP–Rf complex ($\lambda_{ex} = 445$; decay monitored at 520 nm) in CTAB-RMs of $w_0 = 25$ (square) and 33 (circle).

monodispersed RMs, and the observed values are quite consistent with previous literature (Corbeil and Levinger, 2003; Mitra *et al*., 2008). The fluorescence decay transients of RBP fluorescence in the RBP–Rf complex at different hydration levels of CTAB-RM is shown in Figure 5d. The observed quenching in the Trp fluorescence is evident from Table 1 and essentially indicates successful binding of Rf to RBP following the minimum hydration criterion of RBP in a RM (Equation (1)). In fact, the binding of Rf to RBP at these degrees of hydration is very much consistent with the associated absorption and CD spectroscopic data. In Figure 5a, the shoulder at ~490 nm, which is characteristic of Rf binding to RBP, is distinctly observed in both the hydration levels of CTAB-RM. Similarly, the strong CD bands at 445, 370 and 340 nm (Figure 5c) in the visible region for the RBP–Rf complex further supports the hindered rotation of the ribose moiety in the nanospace of RBP. In this situation, one can see the significant quenching of Rf fluorescence in both the steady-state and time-resolved fluorescence spectroscopic data of Figures 5b and 5d, respectively. The observed quenching of Rf fluorescence is well evident from the decay components of Table 2. Notably, the confinement of Rf in CTAB-RM itself quenches the Rf fluorescence (Table 2) and is found to be the quenching effect of bromide ion. In this respect, we monitor the decay transients of Rf in KBr solution and various RMs containing bromide ion, showing the quenching of Rf fluorescence compared with that in buffer (data not shown). It is to be noted that although Rf itself is quenched in the CTAB-RM, the decay time constants of free Rf in CTAB-RM are distinctly different than that present in the protein nanospace (Table 2). Hence, we emphasize that under the confinement of CTAB-RM, Rf present in the nanospace of RBP is free from the bromide quenching effect, and the observed quenching is essentially due to the ultrafast ET in the protein nanospace, which is similar to that in buffer (Table 2).

At this juncture, it is quite essential to discuss on the different behaviour of the flavoprotein under the confinement of RM with different charge types. One can see that the ET of Rf in CTAB-RM occurs in a manner similar to that in buffer, it certainly does not occur under the confinement of anionic AOT-RMs of similar hydration, although the hydration of the protein under confinement enables its binding to Rf. Recent simulation has shown that protein folding/unfolding equilibrium largely depends on the polarity of the confining volume (Tian and Garcia, 2011). The simulation by Griffin *et al*. (2005) suggests that in addition to the confinement effect, surface interaction plays determining role on the dimerization of an off-lattice β-barrel protein. In the present study, the different behaviour of the ET in various RMs suggests that the electrostatic interaction of the RM surface plays a significant role in determining the feasibility of such a process in flavoproteins. Notably in the RM pH ~7.0, RBP is expected to be negatively charged (*p*I of RBP is 4.0; Massolini *et al*., 1995). A study by Lucent *et al*. (2007), using an explicit solvent model, showed that a protein is destabilized when confined by a purely repulsive potential together with solvent. Hence, we emphasize that in the repulsive potential of the confining volume (anionic AOT-RM), the binding site of the protein is so influenced that Rf is unable to complex properly with aromatic amino acids in the protein nanospace. However, under the attractive interaction of the cationic CTAB-RM, the protein conformation is so maintained that Rf can complex properly with aromatic amino acids in the protein nanospace, and ET is feasible with RBP.

CONCLUSION

It has been found that under the confinement of anionic AOT-RM, RBP loses its ability to bind with Rf in RM of $w_0 = 10$; however, it regains its binding capacity and tertiary structure in RM of $w_0 \geq 20$. The reason being that maximum degree of hydration for RBP occurs at $w_0 = 13–16$. Thus, when there is higher volume accessible to a protein and more bulk type water as in the AOT-RM of $w_0 = 20$ and onwards, RBP recovers its tertiary structure as well as binding capacity. Our detailed steady-state and time-resolved spectroscopic data suggest that under the similar size restriction of RM confinement, the biochemical function of RBP–Rf system is distinctly different depending on the hydration and the nature of the RM forming surfactant showing confinement. In anionic AOT-RM, confinement perturbs the ET from RBP to Rf, even at the maximum hydration of the protein. On the other hand, the cationic CTAB-RM resumes such a process with similar confining volume. We believe that because of the electrostatic repulsion of the anionic AOT-RM surface, the cofactor binding site of RBP is so perturbed that Rf is found unable to complex properly with the aromatic amino acids in protein interior. However, the confinement of cationic CTAB-RM resumes such a process with proper binding of Rf in the nanospace of RBP. Thus, both the hydration and surface charge of the confining volume is expected to largely determine the biochemical reaction dynamics like ET in real biological cells. Further studies will expand the present work to a wide range of biochemical reaction systems in different confinements of RMs.

Acknowledgement

SR thanks council of scientific and industrial research (CSIR) for fellowship. The authors thank Department of Science and Technology (DST) for the financial support (SR/SO/BB-15/2007).

REFERENCES

Balzani V (ed.). 2001. Electron transfer in chemistry. Wiley-VCH: Weinheim, Germany.

Bendall DS (ed.). 1996. Protein electron transfer. Bios Scientific, Oxford: U.K.

Bernadó P, de la Torre JG, Pons M. 2004. Macromolecular crowding in biological bystems: hydrodynamics and NMR methods. *J. Mol. Recognit.* **17**(5): 397–407.

Brinker A, Pfeifer G, Kerner MJ, Naylor DJ, Hartl FU, Hayer-Hartl M. 2001. Dual function of protein confinement in chaperonin-assisted protein folding. *Cell* **107**(2): 223–233.

Cheung MS, Thirumalai D. 2007. Effects of crowding and confinement on the structures of the transition state ensemble in proteins. *J. Phys. Chem. B* **111**(28): 8250-8257.

Choi J-D, McCormick DB. 1980. The interaction of flavins with egg white riboflavin-binding protein. *Arch. Biochem. Biophys.* **204**(1): 41–51.

Corbeil EM, Levinger NE. 2003. Dynamics of polar solvation in quaternary microemulsions. *Langmuir* **19**(18): 7264–7270.

Crowley PB, Brett K, Muldoon J. 2008. NMR Spectroscopy reveals cytochrome c–poly(ethylene glycol) interactions. *Chembiochem* **9** (5): 685–688.

Duyvis MG, Hilhorst R, Laane C, Evans DJ, Schmedding DJM. 2002. Role of riboflavin in beer flavor instability: determination of levels of riboflavin and its origin in beer by fluorometric apoprotein titration. *J. Agric. Food Chem.* **50**(6): 1548–1552.

Ellis RJ, Minton AP. 2003. Cell biology: join the crowd. *Nature* **425**(6953): 27–28.

Eryomin AN, Metelitza DI. 1999. Effect of hydration degree of aerosol OT reversed micelles and surfactant concentration in heptane on spectral and catalytic properties of catalase. *Biochemistry (Moscow)* **64**(9): 1049–1060.

Feig M, Sugita Y. 2011. Variable interactions between protein crowders and biomolecular solutes are important in understanding cellular crowding. *J. Phys. Chem. B* **116**(1): 599–605.

Galat A. 1988. Interaction of riboflavin binding protein with riboflavin, quinacrine, chlorpromazine and daunomycin. *Int. J. Biochem.* **20**(9): 1021–1029.

Ghisla S, Kroneck P, Macheroux P, Sund H (eds). 1999. Flavins and Flavoproteins Berlin: Agency for Scientific Pub.

Griffin MA, Friedel M, Shea JE. 2005. Effects of frustration, confinement, and surface interactions on the dimerization of an off-lattice beta-barrel protein. *J. Chem. Phys.* **123**(17): 174707.

Homouz D, Sanabria H, Waxham MN, Cheung MS. 2009. Modulation of calmodulin plasticity by the effect of macromolecular crowding. *J. Mol. Biol.* **391**(5): 933–943.

Isied SS, Ogawa MY, Wishart JF. 1992. Peptide-mediated intramolecular electron transfer: long-range distance dependence. *Chem. Rev.* **92** (3): 381–394.

Jiao M, Li H-T, Chen J, Minton AP, Liang Y. 2010. Attractive protein-polymer interactions markedly alter the effect of macromolecular crowding on protein association equilibria. *Biophys. J.* **99**(3): 914–923.

Li C, Pielak GJ. 2009. Using NMR to distinguish viscosity effects from nonspecific protein binding under crowded conditions. *J. Am. Chem. Soc.* **131**(4): 1368–1369.

Lucent D, Vishal V, Pande VS. 2007. Protein folding under confinement: a role for solvent. *Proc. Natl. Acad. Sci. U. S. A.* **104**(25): 10430–10434.

Luisi PL, Magid LJ. 1986. Solubilisation of enzymes and nucleic acids in hydrocarbon micellar solutions. *CRC Crit. Rev. Biochem.* **20**(4): 409–474.

Lukacs A, Zhao R-K, Haigney A, Brust R, Greetham GM, Towrie M, Tonge PJ, Meech SR. 2012. Excited state structure and dynamics of the neutral and anionic flavin radical revealed by ultrafast transient mid-IR to visible spectroscopy. *J. Phys. Chem. B* **116**(20): 5810–5818.

Massolini G, De Lorenzi E, Ponci MC, Gandini C, Caccialanza G, Monaco HL. 1995. Egg yolk riboflavin binding protein as a new chiral stationary phase in high-Performance liquid chromatography. *J. Chromatogr. A* **704**(1): 55–65.

Mataga N, Chosrowjan H, Shibata Y, Tanaka F, Nishina Y, Shiga K. 2000. Dynamics and mechanisms of ultrafast fluorescence quenching reactions of flavin chromophores in protein nanospace. *J. Phys. Chem. B* **104**(45): 10667–10677.

Mataga N, Chosrowjan H, Taniguchi S, Tanaka F, Kido N, Kitamura M. 2002. Femtosecond fluorescence dynamics of flavoproteins: comparative studies on flavodoxin, its site-directed mutants, and riboflavin binding protein regarding ultrafast electron transfer in protein nanospaces. *J. Phys. Chem. B* **106**(35): 8917–8920.

Mathé J, Aksimentiev A, Nelson DR, Schulten K, Meller A. 2005. Orientation discrimination of single-Stranded DNA inside the α-hemolysin membrane channel. *Proc. Natl. Acad. Sci. U. S. A.* **102**(35): 12377–12382.

McGuffee SR, Elcock AH. 2006. Atomically detailed simulations of concentrated protein solutions: the effects of salt, pH, point mutations, and protein concentration in simulations of 1000-molecule Systems. *J. Am. Chem. Soc.* **128**(37): 12098–12110.

Minton AP. 1983. The Effect of Volume Occupancy upon the Thermodynamic activity of proteins: some biochemical consequences. *Mol. Cell. Biochem.* **55**(2): 119–140.

Minton AP. 1993. Macromolecular crowding and molecular recognition. *J. Mol. Recognit.* **6**(4): 211–214.

Mitra RK, Sinha SS, Pal SK. 2008. Temperature-dependent solvation dynamics of water in sodium bis(2-ethylhexyl)sulfosuccinate/isooctane reverse micelles. *Langmuir* **24**(1): 49–56.

Mittal J, Best RB. 2008. Thermodynamics and kinetics of protein folding under confinement. *Proc. Natl. Acad. Sci. U. S. A.* **105**(51): 20233–20238.

Mondol T, Batabyal S, Pal SK. 2012. Ultrafast electron transfer in the recognition of different DNA sequences by a DNA-binding protein with different dynamical conformations. *J. Biomol. Struct. Dyn.* **30**(3): 362–370.

Müller F(ed.). 1991. Chemistry and biochemistry of flavoenzymes. CRC Press: Boca Raton, FL.

Munishkina LA, Cooper EM, Uversky VN, Fink AL. 2004. The effect of macromolecular crowding on protein aggregation and amyloid fibril formation. *J. Mol. Recognit.* **17**(5): 456–464.

Nissen P, Hansen J, Ban N, Moore PB, Steitz TA. 2000. The structural basis of ribosome activity in peptide bond synthesis. *Science* **289**(5481): 920–930.

Pal SK, Zewail AH. 2004. Dynamics of water in biological recognition. *Chem. Rev.* **104**(4): 2099–2123.

Ping G, Yuan J-M, Sun Z, Wei Y. 2004. Studies of effects of macromolecular crowding and confinement on protein folding and protein stability. *J. Mol. Recognit.* **17**(5): 433–440.

Qin S, Zhou H-X. 2009. Atomistic modeling of macromolecular crowding predicts modest increases in protein folding and binding stability. *Biophys. J.* **97**(1): 12–19.

Rakshit S, Saha R, Verma PK, Mitra RK, Pal SK. 2012. Ultrafast electron transfer in riboflavin binding protein in macromolecular crowding of nano-sized micelle. *Biochimie* doi: 10.1016/j.biochi.2012.08.005.

Rupley JA, Careri G. 1991. Protein hydration and function. *Adv. Prot. Chem.* **41**: 37–172.

Saha R, Rakshit S, Mitra RK, Pal SK. 2012. Microstructure, morphology, and ultrafast dynamics of a novel edible microemulsion. *Langmuir* **28**(22): 8309–8317.

Simpson AA, Tao Y, Leiman PG, Badasso MO, He Y, Jardine PJ, Olson NH, Morais MC, Grimes S, Anderson DL and others. 2000. Structure of the bacteriophage ϕ29 DNA packaging motor. *Nature* **408**(6813): 745–750.

Sinnott M (ed.). 1998. Comprehensive biological catalysis: a mechanistic reference San Diego: Academic.

Stubbe J, van der Donk WA. 1998. Protein radicals in enzyme catalysis. *Chem. Rev.* **98**(2): 705–762.

Tanaka F, Chosrowjan H, Taniguchi S, Mataga N, Sato K, Nishina Y, Shiga K. 2007. Donor – Acceptor distance-dependence of photoinduced electron-transfer rate in flavoproteins. *J. Phys. Chem. B* **111**(20): 5694–5699.

Tian J, Garcia AE. 2011a. Simulation studies of protein folding/unfolding equilibrium under polar and nonpolar confinement. *J. Am. Chem. Soc.* **133**(38): 15157–15164.

Tian JH, Garcia AE. 2011b. Simulations of the confinement of ubiquitin in self-assembled reverse micelles. *J. Chem. Phys.* **134**(22): 225101.

Van Horn WD, Ogilvie ME, Flynn PF. 2009. Reverse Micelle Encapsulation as a Model for Intracellular Crowding. *J. Am. Chem. Soc.* **131**(23): 8030–8039.

Verma PK, Makhal A, Mitra RK, Pal SK. 2009. Role of solvation dynamics in the kinetics of solvolysis reactions in microreactors. *Phys. Chem. Chem. Phys.* **11**(38): 8467–8476.

Verma PK, Saha R, Mitra RK, Pal SK. 2010. Slow water dynamics at the surface of macromolecular assemblies of different morphologies. *Soft Matter* **6**(23): 5971–5979.

Wang W, Xu W-X, Levy Y, Trizac E, Wolynes PG. 2009. Confinement effects on the kinetics and thermodynamics of protein dimerization. *Proc. Natl. Acad. Sci. U. S. A.* **106**(14): 5517–5522.

Wasylewski M. 2000. Binding study of riboflavin-binding protein with riboflavin and its analogues by differential scanning calorimetry. *J. Protein Chem.* **19**(6): 523–528.

Winkler JR. 2006. Long-range electron transfer in biology. John Wiley & Sons, Ltd: Chichester, U.K.

Yeung PSW, Axelsen PH. 2012. The crowded environment of a reverse micelle induces the formation of β-strand seed structures for nucleating Amyloid Fibril Formation. *J. Am. Chem. Soc.* **134**(14): 6061–6063.

Zhang S-Q, Cheung MS. 2007. Manipulating biopolymer dynamics by anisotropic nanoconfinement. *Nano Lett.* **7**(11): 3438–3442.

Zhong D, Zewail AH. 2001. Femtosecond dynamics of flavoproteins: charge separation and recombination in riboflavine (vitamin B2)-binding protein and in glucose oxidase enzyme. *Proc. Natl. Acad. Sci. U. S. A.* **98**(21): 11867–11872.

Zhou H-X. 2004. Protein folding and binding in confined spaces and in crowded solutions. *J. Mol. Recognit.* **17**(5): 368–375.